New constraint on neutrino magnetic moment and neutrino millicharge from LUX-ZEPLIN dark matter search results

M. Atzori Corona[1,2,*] W. M. Bonivento[2,†] M. Cadeddu[2,‡] N. Cargioli[1,2,§] and F. Dordei[2,‖]

[1]*Dipartimento di Fisica, Università degli Studi di Cagliari,*
Complesso Universitario di Monserrato—S.P. per Sestu Km 0.700, 09042 Monserrato (Cagliari), Italy
[2]*Istituto Nazionale di Fisica Nucleare (INFN), Sezione di Cagliari,*
Complesso Universitario di Monserrato—S.P. per Sestu Km 0.700, 09042 Monserrato (Cagliari), Italy

Elastic neutrino-electron scattering represents a powerful tool to investigate key neutrino properties. In view of the recent results released by the LUX-ZEPLIN collaboration, we provide a first determination of the limits achievable on the neutrino magnetic moment and neutrino millicharge, whose effect becomes non-negligible in some beyond the Standard Model theories. In this context, we evaluate and discuss the impact of different approximations to describe the neutrino interaction with atomic electrons. The new LUX-ZEPLIN data allows us to set a very competitive limit on the neutrino magnetic moment when compared to the other laboratory bounds, namely $\mu_\nu^{\text{eff}} < 1.1 \times 10^{-11} \mu_{\text{B}}$ at 90% C.L., which improves by a factor of 2.5 the Borexino collaboration limit and represents the second best world limit after the recent XENONnT result. Moreover, exploiting the so-called equivalent photon approximation, we obtain the most stringent limit on the neutrino millicharge, namely $|q_\nu^{\text{eff}}| < 1.5 \times 10^{-13} e_0$ at 90% C.L., which represents a great improvement with respect to the previous laboratory bounds.

I. INTRODUCTION

Recently, the LUX-ZEPLIN (LZ) Collaboration released the results [1] of the first search for so-called weakly interacting massive particles (WIMPs) [2], one of the most searched candidates to explain dark matter, which is predicted by a large number of theories beyond the Standard Model (SM) [3–5]. The LZ experiment is located at the Sanford Underground Research Facility in Lead, South Dakota. Its core is a dual-phase time projection chamber (TPC) filled with about 10 t of liquid xenon (LXe), of which 7 (5.5) t of the active (fiducial) region. The possible interaction of a WIMP inside the detector produces two detectable signals if the nuclear recoil (NR) is above the ~5 keV$_{\text{nr}}$ threshold, namely scintillation photons (S1) in the detector bulk and a secondary scintillation signal (S2) produced by the ionized electrons that drift thanks to an electric field to the gas pocket on top of the

detector. Both signals are captured by 494 photomultiplier tubes located at the top and the bottom of the TPC. The results reported correspond to 60.3 live days and given that the data are consistent with a background-only hypothesis, permit setting the most stringent limits on the spin-independent and spin-dependent WIMP-nucleon scattering cross section for masses greater than 9 GeV/c^2 [1], as well as new competitive limits on the spin-dependent WIMP-proton cross section.

Among the different background components that characterize a direct dark matter experiment and that are kept into account in the data analysis, there is one due to elastic solar neutrino-electron scattering (νES) inside the TPC. In the LZ analysis, the total number of such electron recoils (ERs) that is found after the combined fit of the background model plus a 30 GeV/c^2 WIMP signal is 27.2 ± 1.6 [1] and represents about 10% of the total background. Such a process is extremely sensitive to some neutrino electromagnetic properties beyond the SM (BSM), as the neutrino magnetic moment (MM) and the neutrino electric charge (EC), usually referred to as millicharge, which can both significantly enhance the νES contribution at low recoil energies [6–11]. Thus, in this work, we revisit the fit to the LZ data allowing for a neutrino MM or a neutrino EC to set competitive limits on these quantities.

During the completion of this work, also the XENONnT collaboration reported its first result based on the analysis of low-energy ER data collected with a dual-phase TPC filled with 4.37 t of LXe fiducial mass and a total exposure

*mattia.atzori.corona@ca.infn.it
†walter.bonivento@ca.infn.it
‡matteo.cadeddu@ca.infn.it
§nicola.cargioli@ca.infn.it
‖francesca.dordei@cern.ch

of 1.16t yr [12]. The experiment obtained the lowest ER background level among current dark matter detectors in its energy range of interest. No excess above the background is found, allowing the collaboration to rule out the well-known XENON-1T excess [11], most probably produced by an unaccounted tritium background. Moreover, they also reported a limit on the neutrino magnetic moment that will be compared to that obtained in this work.

II. THEORETICAL FRAMEWORK

Neutrino-electron elastic scattering is a source of background for direct searches of WIMPs. This background is in principle reducible, but in practice hard to remove completely in experiments that use xenon due to the limited discrimination available between NRs and ERs. Luckily, in the SM its contribution to the total event rate at low recoil energies is rather precisely known and flat with respect to the recoil energy and thus it is usually subtracted in standard dark-matter analyses. However, in certain BSM scenarios, the νES contribution could increase significantly, making it important to investigate this opportunity. Indeed, stronger constraints can be obtained on many neutrino electromagnetic properties [6–10].

The SM νES cross section per xenon atom is obtained multiplying the νES cross section per electron with the effective electron charge of the target atom $Z_{\text{eff}}^{\text{Xe}}(T_e)$ [6,13,14], and for each neutrino flavor ν_ℓ ($\ell = e, \mu, \tau$) is given by

$$\frac{d\sigma_{\nu_\ell}}{dT_\text{e}}(E, T_\text{e}) = Z_{\text{eff}}^{\text{Xe}}(T_e)\frac{G_\text{F}^2 m_e}{2\pi}\left[(g_V^{\nu_\ell} + g_A^{\nu_\ell})^2\right.$$
$$+ (g_V^{\nu_\ell} - g_A^{\nu_\ell})^2\left(1 - \frac{T_e}{E}\right)^2$$
$$\left.- (g_V^{\nu_\ell 2} - g_A^{\nu_\ell 2})\frac{m_e T_e}{E^2}\right], \quad (1)$$

where G_F is the Fermi constant, E is the neutrino energy, m_e is the electron mass, T_e is the electron recoil energy, and the neutrino-flavor dependent electron couplings at tree level are

$$g_V^{\nu_e} = 2\sin^2\theta_W + 1/2, \qquad g_A^{\nu_e} = 1/2, \quad (2)$$

$$g_V^{\nu_{\mu,\tau}} = 2\sin^2\theta_W - 1/2, \qquad g_A^{\nu_{\mu,\tau}} = -1/2. \quad (3)$$

They correspond to $g_V^{\nu_e} = 0.9521$, $g_A^{\nu_e} = 0.4938$, $g_V^{\nu_\mu} = -0.0397$, $g_A^{\nu_{\mu,\tau}} = -0.5062$, and $g_V^{\nu_\tau} = -0.0353$ when taking into account radiative corrections (see Appendix B for further information). Here, θ_W is the weak mixing angle, also known as the Weinberg angle, whose value at zero momentum transfer is $\sin^2\theta_W = 0.23857$ [15] in the $\overline{\text{MS}}$ scheme. The $Z_{\text{eff}}^{\text{Xe}}(T_e)$ term [16,17] quantifies the number of electrons that can be ionized by a certain energy deposit T_e and is needed to correct the cross section derived under the

free electron approximation (FEA) hypothesis. This is especially important for Xe, where one expects a rather big effect from atomic binding [13]. It has been obtained by using the edge energies extracted from photo-absorption data [13,18] (see Appendix A for further information). An alternative method implies the usage of the so-called relativistic random-phase approximation (RRPA) theory [13,19–21]. With respect to the FEA corrected with the stepping function $Z_{\text{eff}}^{\text{Xe}}(T_e)$, RRPA provides an *ab initio* approach able to give an improved description of the atomic many-body effects. In the case of neutrino SM interactions or with additional neutrino MMs, it slightly reduces the νES number of events by an almost constant value as a function of the recoil energy. On the other hand, in the case of neutrino ECs, the low-energy ER spectrum is highly enhanced when using the RRPA formalism with respect to the corrected FEA approach. In this particular case, it is also possible to use the equivalent photon approximation (EPA), which relates the ionization cross section to the photo-absorption one, reproducing closely the RRPA cross section for a milli-charged neutrino [22,23].

The total SM differential cross section includes the contribution from all neutrino flavors keeping into account the oscillation probability in the three-neutrino oscillation scheme and it is

$$\frac{d\sigma_\nu}{dT_\text{e}}(E, T_\text{e}) = P_{ee}\frac{d\sigma_{\nu_e}}{dT_\text{e}} + \sum_{f=\mu,\tau} P_{ef}\frac{d\sigma_{\nu_f}}{dT_\text{e}}, \quad (4)$$

where $P_{ee} = \sin^4\theta_{13} + \cos^4\theta_{13}P^{2\nu}$ [8] is the average survival probability for solar neutrinos reaching the detector when considering the dominant pp and ^{7}Be fluxes, and $P^{2\nu} \simeq 0.55$ [13,15] is the ν_e survival probability in the two-neutrino oscillation scheme. Here, $P_{e\mu} = (1 - P_{ee})\cos^2\theta_{23}$ and $P_{e\tau} = (1 - P_{ee})\sin^2\theta_{23}$ are the transition probabilities. The values of the corresponding mixing angles θ_{13} and θ_{23} were taken from Ref. [15].

III. NEUTRINO MAGNETIC MOMENT

In the SM, neutrinos are considered massless, and therefore neutrino MMs are vanishing. Nevertheless, from the fact that neutrino oscillates, we know that the SM must be extended to give masses to the neutrinos. In the minimal extension of the SM in which neutrinos acquire Dirac masses through the introduction of right-handed neutrinos, the neutrino MM is given by [24–31]

$$\mu_\nu = \frac{3e_0 G_F}{8\sqrt{2}\pi^2}m_\nu \simeq 3.2 \times 10^{-19}\left(\frac{m_\nu}{\text{eV}}\right)\mu_B, \quad (5)$$

where μ_B is the Bohr magneton, m_ν is the neutrino mass, and e_0 is the electric charge. Taking into account the current upper limit on the neutrino mass [15], this value is less than

$\mu_\nu \sim 10^{-18}\mu_B$, which is too small to be observed experimentally. Nevertheless, given that in some BSM scenarios the neutrino MM is predicted to be larger [25], a positive observation would represent a clear signal of physics beyond the minimally extended SM. For this reason, neutrino MM is the most investigated neutrino electromagnetic property, both theoretically and experimentally.

An enhanced MM would increase the neutrino scattering cross sections at low energies on both electrons and nuclei, and thus could be observable by low-threshold detectors, such as the liquid xenon dark matter detectors, as discussed in Refs. [32–35]. By considering the enhancement due to νES, the differential νES cross section that takes into account the contribution of the neutrino MM is given by adding to the SM cross section in Eq. (1) the MM contribution, namely

$$\frac{d\sigma_{\nu_\ell}^{\mathrm{MM}}}{dT_\mathrm{e}}(E, T_\mathrm{e}) = Z_{\mathrm{eff}}^{\mathrm{Xe}}(T_\mathrm{e})\frac{\pi\alpha^2}{m_e^2}\left(\frac{1}{T_\mathrm{e}} - \frac{1}{E}\right)\left|\frac{\mu_{\nu_\ell}}{\mu_\mathrm{B}}\right|^2, \quad (6)$$

where μ_{ν_ℓ} is the effective MM of the flavor neutrino ν_ℓ in elastic scattering (see Ref. [24]).

IV. NEUTRINO MILLICHARGE

It is usually believed that neutrinos are neutral particles. However, in some BSM theories they can acquire a small electric charge (see Ref. [24] and references therein). Within the FEA approach corrected by the stepping function, the millicharged neutrino contribution to the differential ES cross section can be obtained by modifying the neutrino vector coupling $g_V^{\nu_\ell}$ in Eq. (1) through

$$g_V^{\nu_\ell} \to g_V^{\nu_\ell} + \frac{2\sqrt{2}\pi\alpha}{G_F q^2}q_{\nu_\ell}, \quad (7)$$

where q_{ν_ℓ} is the EC associated to the flavor ℓ and $q^2 = -2m_e T_e$ is the momentum transfer in the interaction. Let us note that, in this case, the neutrino EC can interfere with the SM coupling so that the sign of the electric charge is important, while the MM correction is independent of the sign. Given that for low ER energies the momentum transfer is small, the analysis of the LZ data is expected to be particularly promising for millicharged neutrino searches. It is worth mentioning that, although the neutrino MM cross section within the corrected FEA framework is known to be in good agreement with that of *ab initio* theories even for sub-keV ERs, in the same regime the RRPA cross section for a neutrino EC is more than one order of magnitude bigger than that obtained with the corrected FEA [22,23]. In this regard, we can consider the neutrino EC limit obtained within the FEA formalism as a conservative one. Given that it is well known that the EPA scheme reproduces well the RRPA cross section for a millicharged neutrino [22,23], we exploit the EPA formalism in order to go beyond the FEA approach and better

describe the interaction. This improved approach should lead to tighter constraints on the neutrino millicharge. In particular, the EPA cross section for a millicharged ultra-relativistic particle reads [22,23]

$$\frac{d\sigma_{\nu_\ell}}{dT_\mathrm{e}}\bigg|_{\mathrm{EPA}}^{\mathrm{EC}} = \frac{2\alpha}{\pi}\frac{\sigma_\gamma(T_e)}{T_e}\log\left[\frac{E_\nu}{m_\nu}\right]q_{\nu_\ell}^2, \quad (8)$$

where m_ν is the neutrino mass, and $\sigma_\gamma(T_e)$ is the photo-electric cross section by a real photon, which can be extracted from Ref. [18] for Xe. By looking at Eq. (8) it can be seen that the cross section in the EPA approximation is independent of the sign of the electric charge, differently from the case of the FEA approximation. We should underline that, although the EPA approach describes very well the cross section for ER energies below a few keVs, it is known to underestimate the scattering cross section for larger energies where the FEA formalism works better. For this reason, we will rely on the EPA scheme only when its cross section is larger than that of the corrected FEA, following the same procedure adopted in Ref. [36]. In the following, for simplicity, we will refer to this strategy as EPA.

V. DATA ANALYSIS STRATEGY

For the analysis of the LZ dataset, we obtained information on all the quantities used from Ref. [1] and the accompanying data release and supplemental material unless noted otherwise.

The total differential neutrino flux, $dN_{\nu,j}/dE$, is given by the sum of all the different solar neutrino components j as from Refs. [15,37], of which the most relevant for the sensitivity range of LZ are the continuous pp flux and the monochromatic ^{7}Be 861 keV line, even though there are many additional contributions from other mechanisms that are included in the analysis.

In each ER energy bin i, the theoretical νES event number $N_i^{\nu\mathrm{ES}}$ is given by

$$N_i^{\nu\mathrm{ES}} = N(\mathrm{Xe})\int_{T_\mathrm{e}^i}^{T_\mathrm{e}^{i+1}} dT_\mathrm{e}A(T_\mathrm{e})\int_{E_\mathrm{min}(T_\mathrm{e})}^{E_\mathrm{max}} dE\sum_j \frac{dN_{\nu,j}}{dE}(E)$$
$$\times \frac{d\sigma_\nu}{dT_\mathrm{e}}(E, T_\mathrm{e}), \quad (9)$$

where $N(\mathrm{Xe})$ is the number of xenon targets contained in the detector, T_e is the ER kinetic energy, $A(T_\mathrm{e})$ is the energy-dependent detector efficiency, $E_\mathrm{min}(T_\mathrm{e}) = (T_\mathrm{e} + \sqrt{T_\mathrm{e}^2 + 2m_e T_\mathrm{e}})/2$, and $E_\mathrm{max} \sim 2$ MeV. The number of target xenon atoms in the detector is given by $N(\mathrm{Xe}) = N_\mathrm{A}M_\mathrm{det}/M_\mathrm{Xe}$, where N_A is the Avogadro number, $M_\mathrm{det} = 5.5$t is the detector fiducial mass and M_Xe is the average xenon molar mass.

While the LZ collaboration provided the detector efficiency as a function of the NR energy T_nr, the energy
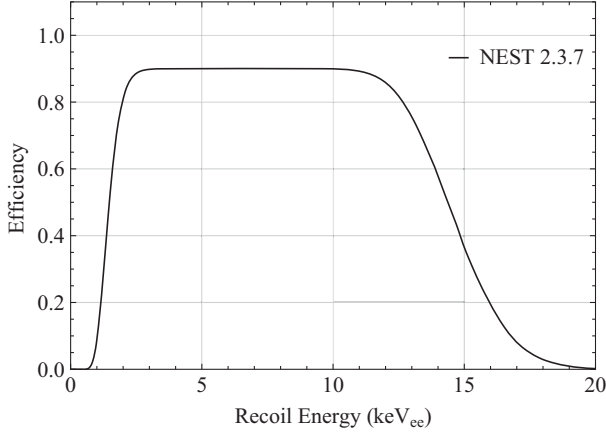
FIG. 1. LZ signal efficiency as a function of the ER energy T_e, obtained from the NEST 2.3.7 software using the details provided by the LZ collaboration.

observed in the detector is the ER energy T_e. For this reason, we derived the detector efficiency as a function of T_e using the NEST [38] 2.3.7 software, following the information provided by the LZ collaboration. The efficiency obtained and used in our analysis is shown in Fig. 1. It is worth mentioning that in a preliminary version of this work [39] we retrieved the ER efficiency curve by converting the NR one through the Lindhard quenching factor [40]. However, this procedure, which was also employed in Ref. [41], neglects the different contributions from ionization and scintillation channels in a dual-phase TPC. Hence, it is not correct and it leads to an incorrect ER efficiency. In particular, the latter procedure overestimates the ER efficiency at low energies, lowering the threshold and hence, leading erroneously to a much stronger sensitivity to the new-physics scenarios considered.

Besides the solar νES, the background components that survive the selection in the region of interest come from different sources, the dominant one being the ERs from radioactive decay of impurities dispersed in the xenon, commonly referred to as β background. Together with a small ($< 1\%$) fraction due to ER from γ rays originating in the detector components and cavern walls, this background represents about 79% of the total one. Other background sources include the naturally occurring isotopes of xenon, which also contribute to ER events, as well as isotopes that are activated cosmogenically, such as ^{127}Xe and ^{37}Ar. Moreover, the NR background has contributions from radiogenic neutrons and coherent elastic neutrino-nucleus scattering (CEνNS) from ^{8}B solar neutrinos. Finally, there is a small component of accidental backgrounds that is also kept into account. Overall, the LZ collaboration reports a background of 333 ± 17 events, of which 27.2 ± 1.6 are due to solar νES, see Table I in Ref. [1].

We performed the analysis of the LZ data using a Poissonian least-squares function [15,42], given that in some energy bins the number of events is small, namely

$$\chi^2 = 2 \sum_{i=1}^{51} \left[(1+\alpha)N_i^{\text{bkg}} + (1+\beta)N_i^{\nu\text{ES}} - N_i^{\exp} \right.$$
$$\left. + N_i^{\exp} \ln\left(\frac{N_i^{\exp}}{(1+\alpha)N_i^{\text{bkg}} + (1+\beta)N_i^{\nu\text{ES}}} \right) \right]$$
$$+ \left(\frac{\alpha}{\sigma_\alpha}\right)^2 + \left(\frac{\beta}{\sigma_\beta}\right)^2, \tag{10}$$

where N_i^{bkg} is the number of residual background events found in the ith bin fit by the LZ collaboration minus that due to solar νES (both extracted from Fig. 6 of Ref. [1]), $N_i^{\nu\text{ES}}$ is the prediction in the ith bin for the νES signal, and $N_i^{\exp}$ is the experimental number of events in the ith bin, also extracted from Fig. 6 of Ref. [1]. The nuisance parameter α takes into account the uncertainty on the neutrino background (with $\sigma_\alpha = 5.1\%$),[1] while β keeps into account the uncertainty on the neutrino flux (with $\sigma_\beta = 7\%$).[2] By using this procedure we ignore that a possible nonzero neutrino MM should also increase the CEνNS contribution from ^{8}B solar neutrinos. However, given that the latter contribution is only 0.15 ± 0.01, we verified that we can safely neglect it. For the future, we note that a lower experimental energy threshold would increase the CEνNS contribution, thus contributing to further strengthening the MM and EC limits.

We highlight that, differently from all the other background sources, the number of ^{37}Ar events is not well constrained theoretically. It is estimated by calculating the exposure of Xe to cosmic rays before it was brought underground, then correcting for the decay time before the search [44]. A flat constraint of 0 to three times (i.e., 288) the estimate of 96 events is imposed because of large uncertainties in the prediction. The fit to the data using this prior finds $52.5^{+9.6}_{-8.9}$ events. In order to keep into account this large uncertainty, we perform a second analysis in which we separate the ^{37}Ar contribution from the total background such that the least-squares function becomes

$$\chi^2_{^{37}\text{Ar}} = 2 \sum_{i=1}^{51} \left[\alpha N_i^{\text{bkg}} + \beta N_i^{\nu\text{ES}} + \delta N_i^{^{37}\text{Ar}} - N_i^{\exp} \right.$$
$$\left. + N_i^{\exp} \ln\left(\frac{N_i^{\exp}}{\alpha N_i^{\text{bkg}} + \beta N_i^{\nu\text{ES}} + \delta N_i^{^{37}\text{Ar}}} \right) \right]$$
$$+ \left(\frac{\alpha - 1}{\sigma_\alpha}\right)^2 + \left(\frac{\beta - 1}{\sigma_\beta}\right)^2 + \left(\frac{\delta - 1}{\sigma_\delta}\right)^2, \tag{11}$$

where N_i^{bkg} is the number of residual background events minus those due to νES and ^{37}Ar as found in the ith electron

---

[1] We note that this procedure ignores the fact that the different background contributions have a different relative uncertainty. However, given that the total background is dominated by the β decays this approximation is valid.

[2] The flux uncertainty is about 7% for ^{7}Be and 0.6% for pp [43], we conservatively use the first one for both fluxes.
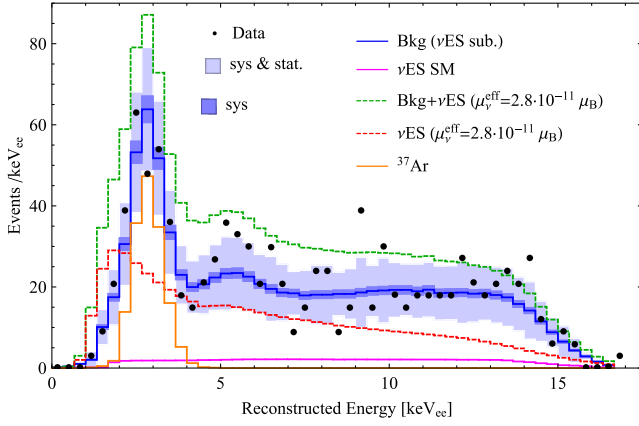
FIG. 2. LZ energy spectrum (black points) as extracted from Fig. 6 of Ref. [1] with superimposed the sum of all background contributions minus the νES contribution (blue solid), the ^{37}Ar contribution (orange), the νES SM prediction (purple), and for illustration purposes the νES with $\mu_\nu^{\text{eff}} = 2.8 \times 10^{-11}\mu_B$, that corresponds to the 90% C.L. limit from BOREXINO [8], with (green dashed) and without (red dashed) the νES subtracted background. The dark blue and the light blue bands represent the systematic and systematic plus statistical uncertainties, respectively, used in this analysis.

recoil energy bin fit by the LZ collaboration, and $N_i^{^{37}\text{Ar}}$ is the number of ^{37}Ar background events found in the ith bin fit by the LZ collaboration, scaled such that the integral is equal to 96 events, as estimated in Ref. [1]. We leave the latter free to vary in the fit with a Gaussian constraint given by the nuisance parameter δ, which takes into account the uncertainty on the ^{37}Ar background, with $\sigma_\delta = 100\%$. In this case, we set $\sigma_\alpha = 13\%$, which is the uncertainty on the expected number of background events provided in Ref. [1] when not considering the ^{37}Ar contribution.

In Fig. 2 we show an example of the νES prediction in presence of a possible neutrino MM for the LZ spectrum compared with the data, the SM νES prediction and the other background components, considering e.g. $\mu_\nu^{\text{eff}} = 2.8 \times 10^{-11}\mu_B$, which corresponds to the previous best limit at 90% confidence level (C.L.) on the neutrino MM from Borexino [8].

VI. RESULTS

Since neutrinos are a mixture of mass eigenstates due to the phenomenon of oscillations, the MM measured for solar νES is an effective value given by

$$\mu_\nu^{2,\text{eff}} = \sum_j \left| \sum_k \mu_{jk} A_k(E_\nu, L) \right|^2, \qquad (12)$$

where μ_{jk} is an element of the neutrino electromagnetic moments matrix and $A_k(E_\nu, L)$ is the amplitude of the k-mass state at the point of scattering [8]. For the Majorana neutrino, only the transition moments are nonzero, while
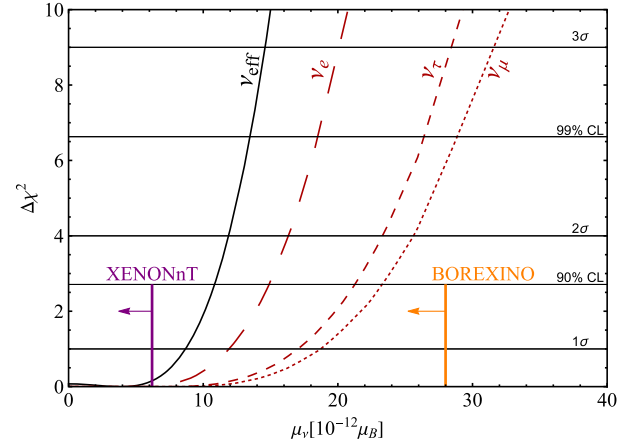
the diagonal elements of the matrix are equal to zero due to CPT conservation. For the Dirac neutrino, all matrix elements may have nonzero values [45].

Similarly, it is possible to define also an effective neutrino millicharge parameter q_ν^{eff} as a combination of the three flavor components.

In Fig. 3 we show the marginal $\Delta\chi^2$s at different confidence levels, obtained using the χ^2 in Eq. (10), for both the effective MM and the marginalization over the three flavor components. The numerical values of the limits derived considering the three different flavors are reported in Table I. At 90% C.L., the bound on the effective neutrino MM obtained in this work is

$$\mu_\nu^{\text{eff}} < 1.1 \times 10^{-11}\mu_B, \qquad (13)$$

with the minimum of the chi-square being $\chi^2_{\min} = 100.0$, which corresponds to an integrated number of $\sim 50\nu$ES events. It can be compared with the limit recently reported by the XENONnT collaboration corresponding to $\mu_\nu^{\text{eff}} < 6.4 \times 10^{-12}\mu_B$ [12], which is about a factor of 2 more

FIG. 3. Marginal $\Delta\chi^2$s for μ_ν^{eff} obtained from the analysis of the LZ data with the χ^2 in Eq. (10) (black solid line) and the marginalized flavor components (dashed red lines). The solid purple (orange) line shows the 90% C.L. upper bound on the effective neutrino MM obtained in the XENONnT [12] (BOREXINO [8]) experiment.

TABLE I. Limits on the neutrino magnetic moment and neutrino millicharge at 90% C.L. obtained with a χ^2 analysis as defined in Eq. (10). For the neutrino millicharge, the limits are reported for both the FEA and the EPA formalism.

	$|\mu_\nu|[\times 10^{-11}\mu_B]$	$q_\nu[\times 10^{-13}e_0]$	
		FEA	EPA
ν_{eff}	<1.1	$[-3.0, 4.7]$	$[-1.5, 1.5]$
ν_e	<1.5	$[-3.6, 6.5]$	$[-2.1, 2.0]$
ν_μ	<2.3	$[-8.9, 8.8]$	$[-3.1, 3.1]$
ν_τ	<2.1	$[-8.1, 8.1]$	$[-2.8, 2.8]$

stringent due to their lower background with respect to LZ. Further neutrino MM analyses exploiting XENONnT data can be found in Refs. [46,47]. These LZ and XENONnT limits, both obtained using a LXe double-phase TPC technology originally designed to search for dark matter and a similar analysis approach, are significantly tighter than the previous laboratory bounds, highlighting the potentiality that such a technique can offer thanks to the low energy threshold and low level of background achieved. Indeed, they can be compared to the limit obtained by the Super-Kamiokande collaboration of $3.6 \times 10^{-10} \mu_B$ (90% C.L.), derived by fitting day/night solar neutrino spectra above 5 MeV. With additional information from other solar neutrino and KamLAND experiments a limit of $1.1 \times 10^{-10} \mu_B$ (90% C.L.) was obtained [48]. The Borexino collaboration reported the previous best current limit on the effective MM by laboratory experiments of $2.8 \times 10^{-11} \mu_B$ (90% C.L.) using the ER spectrum from solar neutrinos [8]. The best MM limit from reactor antineutrinos is $2.9 \times 10^{-11} \mu_B$ (90% C.L.) [49]. Finally, the analysis of the CEνNS data from Dresden-II and COHERENT collaborations permits to set limits on $|\mu_{\nu_e}| < 2.13 \times 10^{-10} \mu_B$ and $|\mu_{\nu_\mu}| < 18 \times 10^{-10} \mu_B$ [6], also exploiting νES. When considering nonlaboratory experiments, the most stringent limits on the neutrino MM of up to $\sim 10^{-12} \mu_B$ come from astrophysical observations [50–52], which however are rather indirect. A complete historical record of limits on the neutrino MM can be found in Ref. [15] and a large collection of existing bounds is summarized in Fig. 5(a). It is possible to see that in our analysis of the LZ data we significantly improve the limits on the electron, muon, and tau neutrino MM compared to the other laboratory bounds.

We checked the impact on the neutrino MM limits of introducing the detector energy resolution in Eq. (9), which is measured to be very precise by the LZ collaboration. For this check, the theoretical spectra were smeared using a Gaussian distribution with an energy-dependent width, which has been determined using an empirical fit of mono-energetic peaks [53]. In particular, for the latter we employed the value reported in Ref. [54], namely $\sigma(T_e) = K/\sqrt{T_e}$, with $K = 0.323 \pm 0.001$. Thanks to the excellent energy resolution achieved by LZ, we verified that its inclusion does not significantly modify the limit obtained. Finally, we investigated the possibility of leaving the ^{37}Ar component free to vary in the fit using a prior similar to that implemented by the LZ collaboration, as defined in Eq. (11). Interestingly, the fit retrieves a number of ^{37}Ar events similar to that found by LZ, namely ~ 48 with $\chi^2_{\min} = 99.6$. Thus, also in this case, the limits do not substantially change and for reference the bound on the effective neutrino MM at 90% C.L. becomes $\mu_\nu^{\mathrm{eff}}(^{37}\mathrm{Ar}) < 1.2 \times 10^{-11} \mu_B$.

As stated in the introduction, the LZ dataset is also very sensitive to a possible neutrino millicharge. In Fig. 4 we present the limits on the neutrino EC obtained in this work within the FEA and EPA formalisms, using the χ^2
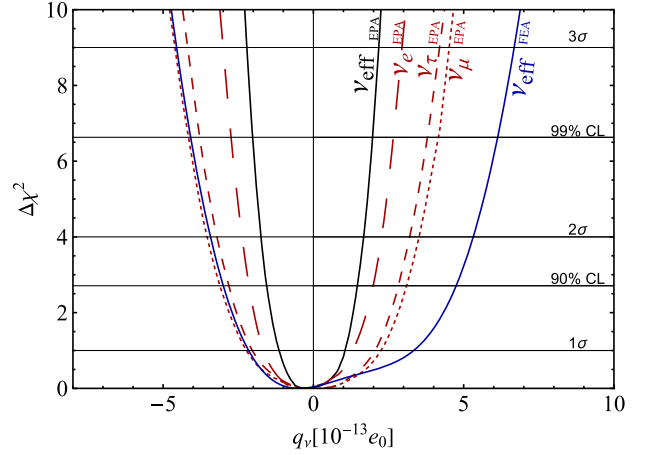

FIG. 4. $\Delta\chi^2$ profiles of the effective (solid black) and flavor dependent (dashed red) neutrino millicharge obtained adopting the EPA formalism. As a comparison, the curve for the effective neutrino millicharge under the FEA approximation is also shown (solid blue).

in Eq. (10). We note that the EPA cross section depends on the neutrino mass, as it can be seen in Eq. (8), which is not yet precisely measured. We used a conservative value of $m_\nu = 1$ eV, which is close to the current laboratory upper bounds on the neutrino mass [15]. On the other hand, we verified that the limit is not significantly modified even when considering smaller values for m_ν. The 90% C.L. bounds on the effective millicharge are

$$\mathrm{FEA}\colon \ -3.0 < q_\nu^{\mathrm{eff}}[10^{-13}e_0] < 4.7, \qquad (14)$$

$$\mathrm{EPA}\colon \ -1.5 < q_\nu^{\mathrm{eff}}[10^{-13}e_0] < 1.5, \qquad (15)$$

the minimum of the chi-square being $\chi^2_{\min} = 100.0$ in both cases. The values for the flavor-dependent neutrino millicharges are summarized in Table I both for the FEA and EPA analyses. It is clear that the limits obtained with the more realistic EPA formalism are much stronger than those obtained within FEA and hence, for simplicity, in Fig. 4 we showed only the effective EC limit for FEA. We note also that the limits obtained in this work with FEA are comparable with those reported in Ref. [46], which exploits the ER energy efficiency derived in this work for the LZ analysis, and are less stringent than those obtained with XENONnT [46,47]. On the other hand, as expected, the limits obtained in this work adopting EPA when analyzing the LZ data are even stronger than the XENONnT limits obtained in Refs. [46,47] that were determined using FEA.

In Fig. 5(b) a collection of existing bounds coming from different experiments is shown. It can be seen that the limits derived in this work using the LZ data and the more realistic EPA formalism significantly improve the
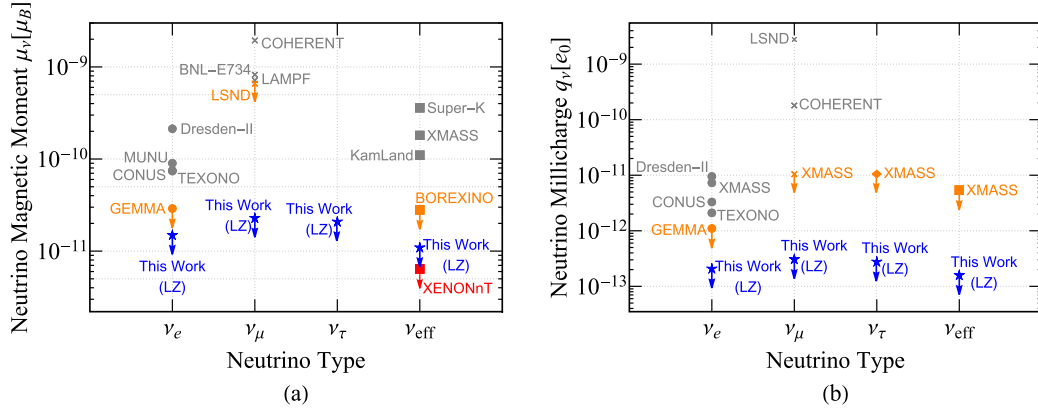
FIG. 5. Summary of existing limits at 90% C.L. on the neutrino magnetic moment (a) and the neutrino millicharge (b) coming from a variety of experiments [6,8,15,24,48,56–63]. The limits are divided in flavor components μ_{ν_e} (q_{ν_e}) (dots), μ_{ν_μ} (q_{ν_μ}) (crosses), and μ_{ν_τ} (q_{ν_τ}) (diamonds) and also the ones on the effective magnetic moment μ_ν^{eff} (q_ν^{eff}) (squares) are shown. In orange, we highlighted the best limits before the LZ data release and in red the XENONnT limit on the MM [12]. The results derived in this work for the effective parameter as well as divided in flavors are shown by the blue stars.

previous best laboratory limits, that for the electron neutrino electric charge was obtained in Ref. [55] by combining TEXONO [56] and GEMMA [57] data, finding $|q_{\nu_e}| < 1.0 \times 10^{-12} e_0$. We expect, however, that adopting the EPA or the RRPA formalism to analyse the XENONnT data would allow us to further constrain the limit on this fundamental quantity. This investigation will be carried out in a future work.

For completeness, also in this case we investigated the impact of repeating the analysis leaving the ^{37}Ar component free to vary, similarly to what was done for the neutrino MM limits. In this case, the bounds on the effective neutrino millicharge become

$$\text{FEA}: \quad -3.3 < q_\nu^{\text{eff}}(^{37}\text{Ar})[10^{-13} e_0] < 5.0, \quad (16)$$

$$\text{EPA}: \quad -1.6 < q_\nu^{\text{eff}}(^{37}\text{Ar})[10^{-13} e_0] < 1.5, \quad (17)$$

with the minimum of the chi-square being $\chi^2_{\text{min}} = 99.6$ in both cases. As before, leaving the ^{37}Ar component free to vary does not impact significantly the results. Moreover, we foresee that in the future this should be even less problematic given that ^{37}Ar has a half-life of about 35 days and thus should be not present in future LZ data samples.

VII. CONCLUSIONS

In this paper, we describe the search for a possible neutrino electromagnetic interaction by exploiting elastic solar neutrino-electron scattering data provided by the LUX-ZEPLIN Collaboration. By using 331.65 t days of data we searched for effects of the neutrino magnetic moment and neutrino millicharge by looking for distortions in the shape and normalization of the electron recoil spectrum. At 90% C.L. we obtain a competitive upper limit on the effective neutrino magnetic moment, namely $\mu_\nu^{\text{eff}} < 1.1 \times 10^{-11} \mu_{\text{B}}$, which is second only to the recent XENONnT limit. We also determined the limits considering the three different neutrino flavors separately, so the results obtained in this work can be easily compared also with experiments not sensitive to solar neutrinos. To fully exploit the potentiality of the LZ data, we also derived intriguing constraints on the neutrino millicharge discussing the impact of different interaction models, namely the FEA and the more robust and reliable EPA, showing that the EPA approach leads to much more stringent constraints. Using EPA, we obtain the current best limit on the effective neutrino millicharge $|q_\nu^{\text{eff}}| < 1.5 \times 10^{-13} e_0$, improving significantly with respect to previous bounds. Also in this scenario, we derived the limits considering the three different flavor components, achieving also in this case the current best limits.

APPENDIX A: THE $Z_{\text{eff}}^{\mathcal{A}}(T_e)$ TERM

The $Z_{\text{eff}}^{\mathcal{A}}(T_e)$ term [16,17], which quantifies the number of electrons that can be ionized by a certain energy deposit T_e, is given for xenon in Table II. It has been obtained by using the edge energies extracted from photoabsorption data [18].

TABLE II.   The effective electron charge of the target atom, $Z_{\mathrm{eff}}^{\mathrm{Xe}}(T_e)$.

$$Z_{\mathrm{eff}}^{\mathrm{Xe}} = \begin{cases} 54, & T_e > 34.561 \text{ keV} \\ 52, & 34.561 \text{ keV} \geq T_e > 5.4528 \text{ keV} \\ 50, & 5.4528 \text{ keV} \geq T_e > 5.1037 \text{ keV} \\ 48, & 5.1037 \text{ keV} \geq T_e > 4.7822 \text{ keV} \\ 44, & 4.7822 \text{ keV} \geq T_e > 1.1487 \text{ keV} \\ 42, & 1.1487 \text{ keV} \geq T_e > 1.0021 \text{ keV} \\ 40, & 1.0021 \text{ keV} \geq T_e > 0.9406 \text{ keV} \\ 36, & 0.9406 \text{ keV} \geq T_e > 0.689 \text{ keV} \\ 32, & 0.689 \text{ keV} \geq T_e > 0.6764 \text{ keV} \\ 26, & 0.6764 \text{ keV} \geq T_e > 0.2132 \text{ keV} \\ 24, & 0.2132 \text{ keV} \geq T_e > 0.1467 \text{ keV} \\ 22, & 0.1467 \text{ keV} \geq T_e > 0.1455 \text{ keV} \\ 18, & 0.1455 \text{ keV} \geq T_e > 0.0695 \text{ keV} \\ 14, & 0.0695 \text{ keV} \geq T_e > 0.0675 \text{ keV} \\ 10, & 0.0675 \text{ keV} \geq T_e > 0.0233 \text{ keV} \\ 4, & 0.0233 \text{ keV} \geq T_e > 0.0134 \text{ keV} \\ 2, & 0.0134 \text{ keV} \geq T_e > 0.0121 \text{ keV} \\ 0, & T_e \leq 0.0121 \text{ keV} \end{cases}$$

APPENDIX B: NEUTRINO-ELECTRON COUPLING DETERMINATION

In order to study the neutrino-electron scattering process, it is necessary to study in detail the calculation of the couplings, taking into account the radiative corrections. The latter are implemented following the formalism given in Ref. [64]. In particular, the ℓ flavor neutrino right and left couplings to fermions, with $f = e$, are given by

$$g_{LL}^{\nu_\ell f} = \rho\left[-\frac{1}{2} - Q_f \hat{s}_0^2 + \boxtimes_{ZZ}^{fL}\right] - Q_f \varnothing_{\nu_\ell W} + \square_{WW}, \quad \text{(B1)}$$

$$g_{LR}^{\nu_\ell f} = -\rho[Q_f \hat{s}_0^2 + \boxtimes_{ZZ}^{fR}] - Q_f \varnothing_{\nu_\ell W}. \quad \text{(B2)}$$

In these relations, $\rho = 1.00063$ represents a low-energy correction for neutral-current processes and Q_f is the

fermion charge. Here $\hat{s}_0^2 = \sin^2 \vartheta_W^{\mathrm{SM}}$, which keeps the same value for $\mu < \mathcal{O}(0.1 \text{ GeV})$. The other corrections inserted come from different contributions, such as the charge radii ($\varnothing_{\nu_\ell W}$), and EW box diagrams ($\boxtimes_{ZZ}^{fX}$, $\square_{WW}$). They can be expressed as

$$\varnothing_{\nu_\ell W} = -\frac{\alpha}{6\pi}\left(\ln\frac{M_W^2}{m_\ell^2} + \frac{3}{2}\right), \quad \text{(B3)}$$

$$\square_{WW} = -\frac{\hat{\alpha}_Z}{2\pi\hat{s}_Z^2}\left[1 - \frac{\hat{\alpha}_s(M_W)}{2\pi}\right], \quad \text{(B4)}$$

$$\boxtimes_{ZZ}^{fX} = -\frac{3\hat{\alpha}_Z}{8\pi\hat{s}_Z^2\hat{c}_Z^2}(g_{LX}^{\nu_\ell f})^2\left[1 - \frac{\hat{\alpha}_s(M_Z)}{\pi}\right], \quad \text{(B5)}$$

where $X \in \{L, R\}$ and $\hat{\alpha}_Z \equiv \alpha(M_Z)$. Note that in Eq. (B5) all the $(g_{LX})^{\nu_\ell f}$ are evaluated at lowest order but replacing $\hat{s}_0^2$ by $\hat{s}_Z^2$ and are given by $g_{LL}^{\nu_\ell e} = -\frac{1}{2} + \hat{s}_Z^2$ and $g_{LR}^{\nu_\ell e} = \hat{s}_Z^2$. For neutrino-electron scattering the couplings are given by

$$g_V^{\nu_\ell e} = \rho\left(-\frac{1}{2} + 2\hat{s}_0^2\right) + \square_{WW} + 2\varnothing_{\nu_\ell W} + \rho(\boxtimes_{ZZ}^{eL} - \boxtimes_{ZZ}^{eR}),$$
$$\text{(B6)}$$

$$g_A^{\nu_\ell e} = \rho\left(-\frac{1}{2} + \boxtimes_{ZZ}^{eL} + \boxtimes_{ZZ}^{eR}\right) + \square_{WW}, \quad \text{(B7)}$$

where $g_A^{\nu_\ell e} = g_{LL}^{\nu_\ell e} - g_{LR}^{\nu_\ell e}$.

For the numerical SM evaluation we assume the values from Refs. [15,65], namely $\hat{s}_0^2 = 0.23857$, $\hat{s}_Z^2 = 0.23121$, $\alpha_s(M_W) = 0.123$, $\alpha_s(M_Z) = 0.1185$, and $\hat{\alpha}_Z^{-1} = 127.952$. We thus obtain the couplings $g_V^{\nu_e} = 0.9521$, $g_A^{\nu_e} = 0.4938$, $g_V^{\nu_\mu} = -0.0397$, $g_A^{\nu_{\mu,\tau}} = -0.5062$, and $g_V^{\nu_\tau} = -0.0353$ that take into account all radiative corrections. We note that, for the ν_e coupling, an unity factor has been added to the result in order to take into account the charge current contribution.

[1] J. Aalbers *et al.*, First dark matter search results from the LUX-ZEPLIN (LZ) experiment, arXiv:2207.03764.

[2] B. W. Lee and S. Weinberg, Cosmological Lower Bound on Heavy Neutrino Masses, Phys. Rev. Lett. **39,** 165 (1977).

[3] G. Bertone and D. Hooper, History of dark matter, Rev. Mod. Phys. **90,** 045002 (2018).

[4] J. Billard *et al.*, Direct detection of dark matter—APPEC committee report*, Rep. Prog. Phys. **85,** 056201 (2022).

[5] D. S. Akerib *et al.*, Snowmass 2021 cosmic frontier dark matter direct detection to the neutrino fog, arXiv:2203.08084.

[6] M. A. Corona, M. Cadeddu, N. Cargioli, F. Dordei, C. Giunti, Y. F. Li, C. A. Ternes, and Y. Y. Zhang, Impact of the Dresden-II and COHERENT neutrino scattering data on neutrino electromagnetic properties and electroweak physics, J. High Energy Phys. 09 (2022) 164.

[7] P. Coloma, I. Esteban, M. C. Gonzalez-Garcia, L. Larizgoitia, F. Monrabal, and S. Palomares-Ruiz, Bounds on new physics with data of the Dresden-II reactor experiment and COHERENT, J. High Energy Phys. 05 (2022) 037.

[8] M. Agostini *et al.* (Borexino Collaboration), Limiting neutrino magnetic moments with Borexino Phase-II solar neutrino data, Phys. Rev. D **96,** 091103 (2017).

[9] O. G. Miranda, D. K. Papoulias, M. Tórtola, and J. W. F. Valle, XENON1T signal from transition neutrino magnetic moments, Phys. Lett. B **808,** 135685 (2020).

[10] W. Grimus, M. Maltoni, T. Schwetz, M. A. Tortola, and J. W. F. Valle, Constraining Majorana neutrino electromagnetic properties from the LMA-MSW solution of the solar neutrino problem, Nucl. Phys. **B648,** 376 (2003).

[11] E. Aprile *et al.* (XENON Collaboration), Excess electronic recoil events in XENON1T, Phys. Rev. D **102,** 072004 (2020).

[12] E. Aprile *et al.* (XENON Collaboration), Search for New Physics in Electronic Recoil Data from XENONnT, Phys. Rev. Lett. **129,** 161805 (2022).

[13] J.-W. Chen, H.-C. Chi, C.-P. Liu, and C.-P. Wu, Low-energy electronic recoil in Xenon detectors by solar neutrinos, Phys. Lett. B **774,** 656 (2017).

[14] K. A. Kouzakov and A. I. Studenikin, Theory of neutrino-atom collisions: The history, present status and BSM physics, Adv. High Energy Phys. **2014,** 569409 (2014).

[15] P. A. Zyla *et al.* (Particle Data Group), Review of particle physics, Prog. Theor. Exp. Phys. **2020,** 083C01 (2020), and 2021 update.

[16] L. A. Mikaelyan, Investigation of neutrino properties in experiments at nuclear reactors: Present status and prospects, Phys. At. Nucl. **65,** 1173 (2002).

[17] S. A. Fayans, L. A. Mikaelyan, and V. V. Sinev, Weak and magnetic inelastic scattering of anti-neutrinos on atomic electrons, Phys. At. Nucl. **64,** 1475 (2001).

[18] B. Henke, E. Gullikson, and J. Davis, X-ray interactions: Photoabsorption, scattering, transmission, and reflection at $e = 50$–$30{,}000$ ev, $z = 1$–92, At. Data Nucl. Data Tables **54,** 181 (1993).

[19] K. N. Huang and W. R. Johnson, Multiconfiguration relativistic random-phase approximation. Theory, Phys. Rev. A **25,** 634 (1982).

[20] K.-N. Huang, Relativistic many-body theory of atomic transitions. The relativistic equation-of-motion approach, Phys. Rev. A **26,** 734 (1982).

[21] J.-W. Chen, H.-C. Chi, K.-N. Huang, C. P. Liu, H.-T. Shiao, L. Singh, H. T. Wong, C.-L. Wu, and C.-P. Wu, Atomic ionization of germanium by neutrinos from an *ab initio* approach, Phys. Lett. B **731,** 159 (2014).

[22] J.-W. Chen, H.-C. Chi, K.-N. Huang, H.-B. Li, C. P. Liu, L. Singh, H. T. Wong, C.-L. Wu, and C.-P. Wu, Constraining neutrino electromagnetic properties by germanium detectors, Phys. Rev. D **91,** 013005 (2015).

[23] C.-C. Hsieh, L. Singh, C.-P. Wu, J.-W. Chen, H.-C. Chi, C. P. Liu, M. K. Pandey, and H. T. Wong, Discovery potential of multiton xenon detectors in neutrino electromagnetic properties, Phys. Rev. D **100,** 073001 (2019).

[24] C. Giunti and A. Studenikin, Neutrino electromagnetic interactions: A window to new physics, Rev. Mod. Phys. **87,** 531 (2015).

[25] C. Giunti, K. A. Kouzakov, Y.-F. Li, A. V. Lokhov, A. I. Studenikin *et al.*, Electromagnetic neutrinos in terrestrial experiments and astrophysics, Ann. Phys. (Berlin) **528,** 198 (2016).

[26] K. Fujikawa and R. E. Shrock, Magnetic Moment of a Massive Neutrino and Neutrino-Spin Rotation, Phys. Rev. Lett. **45,** 963 (1980).

[27] J. Schechter and J. W. F. Valle, Majorana neutrinos and magnetic fields, Phys. Rev. D **24,** 1883 (1981); **25,** 283(E) (1982).

[28] B. Kayser, Majorana neutrinos and their electromagnetic properties, Phys. Rev. D **26,** 1662 (1982).

[29] J. F. Nieves, Electromagnetic properties of majorana neutrinos, Phys. Rev. D **26,** 3152 (1982).

[30] P. B. Pal and L. Wolfenstein, Radiative decays of massive neutrinos, Phys. Rev. D **25,** 766 (1982).

[31] R. E. Shrock, Electromagnetic properties and decays of dirac and majorana neutrinos in a general class of gauge theories, Nucl. Phys. **B206,** 359 (1982).

[32] G. Yuan Huang and S. Zhou, Constraining neutrino lifetimes and magnetic moments via solar neutrinos in the large xenon detectors, J. Cosmol. Astropart. Phys. 02 (2019) 024.

[33] K. S. Babu, S. Jana, and M. Lindner, Large neutrino magnetic moments in the light of recent experiments, J. High Energy Phys. 10 (2007) 040.

[34] T. Schwemberger and T.-T. Yu, Detecting beyond the standard model interactions of solar neutrinos in low-threshold dark matter detectors, Phys. Rev. D **106,** 015002 (2022).

[35] Y.-F. Li and S.-y. Xia, Probing neutrino magnetic moments and the XENON1T excess with coherent elastic solar neutrino scattering, Phys. Rev. D **106,** 095022 (2022).

[36] L. Singh *et al.* (TEXONO Collaboration), Constraints on millicharged particles with low threshold germanium detectors at Kuo-Sheng reactor neutrino laboratory, Phys. Rev. D **99,** 032009 (2019).

[37] E. Vitagliano, I. Tamborra, and G. Raffelt, Grand unified neutrino spectrum at earth: Sources and spectral components, Rev. Mod. Phys. **92,** 045006 (2020).

[38] M. Szydagis, N. Barry, K. Kazkaz, J. Mock, D. Stolp, M. Sweany, M. Tripathi, S. Uvarov, N. Walsh, and M. Woods, NEST: A comprehensive model for scintillation yield in liquid xenon, J. Instrum. **6,** P10002 (2011).

[39] M. Atzori Corona, W. M. Bonivento, M. Cadeddu, N. Cargioli, and F. Dordei, New constraint on neutrino magnetic moment from LZ dark matter search results, arXiv:2207.05036v2.

[40] J. Lindhard, V. Nielsen, M. Scharff, and P. V. Thomsen, Integral equations governing radiation effects. (Notes on atomic collisions, III), Kgl. Danske Videnskab., Selskab. Mat. Fys. Medd. **33** (1963).

[41] T. N. Maity and R. Laha, Cosmic-ray boosted dark matter in Xe-based direct detection experiments, arXiv:2210.01815.

[42] S. Baker and R. D. Cousins, Clarification of the use of chi square and likelihood functions in fits to histograms, Nucl. Instrum. Methods Phys. Res. **221,** 437 (1984).

[43] A. Serenelli, Alive and well: A short review about standard solar models, Eur. Phys. J. A **52,** 78 (2016).

[44] J. Aalbers *et al.* (LUX-ZEPLIN Collaboration), Cosmogenic production of Ar37 in the context of the LUX-ZEPLIN experiment, Phys. Rev. D **105,** 082004 (2022).

[45] K. A. Kouzakov and A. I. Studenikin, Electromagnetic properties of massive neutrinos in low-energy elastic neutrino-electron scattering, Phys. Rev. D **95**, 055013 (2017); **96**, 099904(E) (2017).

[46] K. A. ShivaSankar, A. Majumdar, D. K. Papoulias, H. Prajapati, and R. Srivastava, First results of LZ and XENONnT: A comparative study of neutrino properties and light mediators, arXiv:2208.06415.

[47] A. N. Khan, New limits on neutrino electromagnetic interactions and light new physics with XENONnT, Phys. Lett. B **837**, 137650 (2023).

[48] D. W. Liu *et al.* (Super-Kamiokande Collaboration), Limits on the Neutrino Magnetic Moment Using 1496 Days of Super-Kamiokande-I Solar Neutrino Data, Phys. Rev. Lett. **93**, 021802 (2004).

[49] A. G. Beda *et al.* (GEMMA Collaboration), Gemma experiment: The results of neutrino magnetic moment search, Phys. Part. Nucl. Lett. **10**, 143 (2013).

[50] S. Arceo-Díaz, K.-P. Schroeder, K. Zuber, and D. Jack, Constraint on the magnetic dipole moment of neutrinos by the tip-RGB luminosity in centauri, Astropart. Phys. **70**, 1 (2015).

[51] S. A. Díaz, K.-P. Schröder, K. Zuber, D. Jack, and E. E. B. Barrios, Constraint on the axion-electron coupling constant and the neutrino magnetic dipole moment by using the tip-RGB luminosity of fifty globular clusters, arXiv:1910.10568.

[52] A. H. Córsico, L. G. Althaus, M. M. Miller Bertolami, S. O. Kepler, and E. García-Berro, Constraining the neutrino magnetic dipole moment from white dwarf pulsations, J. Cosmol. Astropart. Phys. 08 (2014) 054.

[53] D. S. Akerib *et al.* (LZ Collaboration), The LUX-ZEPLIN (LZ) Experiment, Nucl. Instrum. Methods Phys. Res., Sect. A **953**, 163047 (2020).

[54] G. Pereira, Energy resolution of the LZ detector for high-energy electronic recoils, *Proceeding of the 5th XeSAT Conference* (2022), https://indico.in2p3.fr/event/20879/contributions/109640/attachments/70740/100409/GuilhermePereira_%20Energy%20resolution%20of%20LZ%20detector%20for%20High%20Energy%20Electronic%20Recoils.pdf.

[55] J.-W. Chen, H.-C. Chi, H.-B. Li, C. P. Liu, L. Singh, H. T. Wong, C.-L. Wu, and C.-P. Wu (TEXONO Collaboration), Constraints on millicharged neutrinos via analysis of data from atomic ionizations with germanium detectors at sub-keV sensitivities, Phys. Rev. D **90**, 011301 (2014).

[56] H. T. Wong *et al.* (TEXONO Collaboration), A search of neutrino magnetic moments with a high-purity germanium detector at the Kuo-Sheng nuclear power station, Phys. Rev. D **75**, 012001 (2007).

[57] A. Beda, V. Brudanin, V. Egorov, D. Medvedev, V. Pogosov *et al.*, The results of search for the neutrino magnetic moment in GEMMA experiment, Adv. High Energy Phys. **2012**, 350150 (2012).

[58] H. Bonet *et al.* (CONUS Collaboration), First upper limits on neutrino electromagnetic properties from the CONUS experiment, Eur. Phys. J. C **82**, 813 (2022).

[59] Z. Daraktchieva *et al.* (MUNU Collaboration), Final results on the neutrino magnetic moment from the MUNU experiment, Phys. Lett. B **615**, 153 (2005).

[60] R. C. Allen, H. H. Chen, P. J. Doe, R. Hausammann, W. P. Lee, X. Q. Lu, H. J. Mahler, M. E. Potter, K. C. Wang, T. J. Bowles, R. L. Burman, R. D. Carlini, D. R. F. Cochran, J. S. Frank, E. Piasetzky, V. D. Sandberg, D. A. Krakauer, and R. L. Talaga, Study of electron-neutrino—electron elastic scattering at Lampf, Phys. Rev. D **47**, 11 (1993).

[61] L. Ahrens, S. Aronson, P. Connolly, B. Gibbard, M. Murtagh *et al.*, Determination of electroweak parameters from the elastic scattering of muon-neutrinos and antineutrinos on electrons, Phys. Rev. D **41**, 3297 (1990).

[62] L. B. Auerbach *et al.* (LSND Collaboration), Measurement of electron—neutrino—electron elastic scattering, Phys. Rev. D **63**, 112001 (2001).

[63] K. Abe *et al.* (XMASS Collaboration), Search for exotic neutrino-electron interactions using solar neutrinos in XMASS-I, Phys. Lett. B **809**, 135741 (2020).

[64] J. Erler and S. Su, The weak neutral current, Prog. Part. Nucl. Phys. **71**, 119 (2013).

[65] J. Alitti *et al.* (UA2 Collaboration), A determination of the strong coupling constant alpha-s from W production at the CERN p anti-p collider, Phys. Lett. B **263**, 563 (1991).